Results in Materials 8 (2020) 100151

Contents lists available at ScienceDirect

Results in Materials

journal homepage: www.journals.elsevier.com/results-in-materials

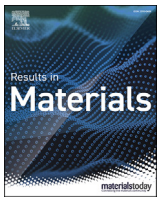

Formulation of a Generalized Unit Cell and its Application to Shot Peening Simulation

Christoph H. Richter [a,*], Patrick Gerken [a], Gerd Telljohann [b]

[a] Hochschule Osnabrück, Albrechtstr. 30, 49076, Osnabrück, Germany
[b] DYNATEC GmbH, Adam-Opel-Str. 4, 38112, Braunschweig, Germany

ARTICLE INFO

Keywords:
Generalized periodicity
Unit cell
Shot peening intensity
Pre-stress shot peening
Fatigue-relevant scatter

ABSTRACT

The simulation of the residual stress field achieved by shot peening cannot be carried out on component-large models. Hence, an efficient unit cell model for the simulation of the shot peening process is developed. The model allows both, the simple inclusion of a pre-stress and the evaluation of the up-arching of the Almen strip. For this purpose, generalized coupling constraints for the periodic boundaries of the unit cell are developed. These allow for displacement and rotation of the coupled boundaries relative to each other. In the coupling constraints, this is accomplished by respective variables, which can either be prescribed to the analysis or read out as a result from the analysis. Hence, the unit cell can expand, shear, bend and twist under driving forces like, e. g., residual stresses or thermal effects. At the same time, deformations of the cell's periodic boundary pairs are kept congruent by the generalized coupling. The ability to cover expansion is novel regarding known periodic boundary conditions. Also, the application of a generalized unit cell to shot peening is new.

Results obtained with the generalized unit cell are displayed, demonstrating its capabilities: A fundamental analysis of the residual stress field from shot peening shows inhomogeneities at a fatigue relevant level to be inevitable. A validation of the model was done by comparison with experimental Almen strip shot peening tests reported in literature. Shot peening under pre-stress is demonstrated and its results in terms of residual stress are evaluated. The application of the generalized unit cell is not limited to shot peening.

1. Introduction

The manufacturing process of strengthening by cold forming has been known for a very long time. Shot peening, in which preferably spherical shot is thrown repeatedly and randomly at the component's surface, is such a process. The impact of the shot on the component causes a thin layer of residual compressive stresses near the surface, typically a few tenth of a millimeter thick. These are superimposed by the stresses resulting from the load. The result is a lower stress level which, with regard to material fatigue, results in a reduced mean stress and thus increased fatigue durability. The mechanism consists in a hindrance of the shear stress driven dislocation sliding by a lowered normal stress perpendicular to the slip planes. In the case of a small crack reaching into the compressive residual stress layer, this results in crack-relieving and crack-closing effects that may prevent further crack growth. The reduced stress level is also beneficial in the case of stress corrosion cracking. Due to its strengthening effect, shot peening is well established in a wide variety of mechanical engineering sectors, such as turbomachinery and gear manufacturing [1, 2]. In additive manufacturing, e. g. of laser-sintered machine components, it can at least partially compensate for any deficiencies (roughness, tensile residual stresses) created in the surface of the component during the manufacturing process [3, 4].

To optimize the component performance, a simulation of the shot peening process is necessary to gain insight into the residual stress field and its effect on fatigue durability. Unit cell models are employed as these have a minimum representative section of the component, reducing calculation effort or allowing the simulation at all. The cut boundaries of the cell are coupled to represent periodicity, usually prescribing identical displacement for congruent nodes. It is the aim to develop a generalized unit cell, to validate it and to demonstrate its efficiency in applications.

Exposed to loads a component may undergo expansion and/or bending and/or torsion. The generalized unit cell shall be able to represent this behavior. Therefore, the periodic coupling equations shown in this paper take into account expansion and rotation of the cell's boundaries relative to each other. At the same time, the boundaries have to keep identical shape. The expansion and rotation can either be

* Corresponding author.
E-mail address: c.h.richter@hs-osnabrueck.de (C.H. Richter).

https://doi.org/10.1016/j.rinma.2020.100151
Received in revised form 20 October 2020; Accepted 20 October 2020
Available online 9 November 2020

prescribed to the analysis or read out as a result from the analysis. This is a useful feature of the proposed unit cell. Prescribing expansion and bending is used e. g. for the simulation of shot peening under pre-stress; reading out expansion and bending is employed, e. g., to evaluate the deformation of an Almen strip under residual stress.

1.1. Technology and Effect of Shot Peening

Process Description and Overview. In shot peening, mostly spherical bodies with dimensions ranging from a few tenths to a few millimeters, depending on the application, are shot with a certain speed (typically 50–100 m/s) at the surface of the material to be treated. A section of the surface area can be seen in Fig. 1. The bombardment must be repeated within the random process until the entire surface is hit uniformly. Common materials for the shot include steel, ceramic and glass [5–7]. Accelerating the balls with a conveying air flow or with an impeller is state of the art. To control the shot velocity the amount of conveying air or the impeller speed can be varied, respectively. Shot peening was first used commercially by Zimmerli [8] and Almen [9] for valve springs of piston engines in the late 1920s.

Mechanism of Residual Stresses. The kinetic energy of a ball is so great that its impact causes plastic deformations in the near-surface areas of the material. Hence, this material is strengthened and compressive residual stresses are introduced in a thin layer. The plastic deformations are such that fibers aligned parallel to the surface would expand if they could be freed from the material. Fig. 1 shows fibers of originally identical length with their free lengths at different depths below the surface after shot peening. At a certain depth, the material is practically unchanged through the process. The change in length of the vertical fibers is comparatively small. The plastically elongated fibers are pushed back by the underlying bulk material, which was deformed only elastically during the peening process. Therefore, compressive stresses emanate in planes parallel to the surface. Fig. 1 shows the graph of the compressive stress over the depth qualitatively. Below the residual compressive stress zone, there is a zone of moderate tensile stresses resulting from the internal equilibrium of forces. Cracks that develop and grow into depth thereby experience crack-closing forces from the residual stresses; hence, crack growth is impeded [10]. The described effects of shot peening can be amplified by exposing the surface to an elastic tensile pre-stress during the shot peening. This pre-stress is induced with a static load of the component.

Quality Control with Almen Strip. Besides ball properties like material, hardness and size, the speed of the ball is a central process parameter. In addition, the number of impacts per surface element is just as important. To control both quantities, an accompanying sample, the Almen strip, is peened during the process. This specimen is a flat fixed sheet metal strip or circular blank made of spring steel (SAE 1070) [1, 11]. In contrast to a component, the Almen strip arches up measurably under the effect of the residual stresses after releasing its fixation [12]. This is due to its small moments of inertia about the bending axes. As a result of bending upwards, the level of the compressive stresses in the Almen strip decreases. The arc height of the bent Almen strip over the course of impacts or time, $A(t)$, allows to conclude on the impact intensity viz. on the speed of the balls. The impressions due to balls impacting on the surface provide information about the number of area-specific impacts. The fraction of the surface hit is the coverage ratio D. [13]

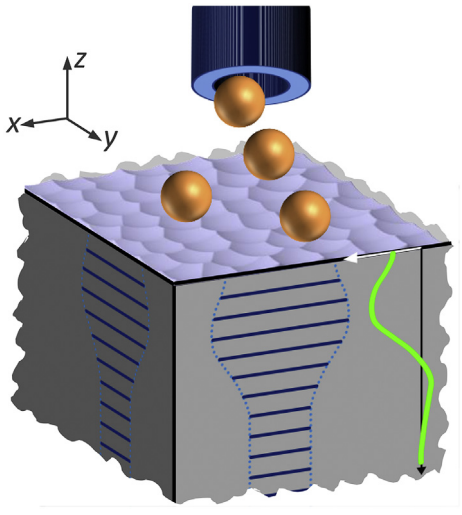

Fig. 1. Fibre lengths (blue lines) as altered due to shot peening and the resulting compressive stresses over the depth (green curve). Concave impressions from the impacting spheres can be seen on the surface (the proportions are not to scale).

Process Parameters. The determination of the process parameters like the shot, conveying air pressure and peening time is an iterative and experimental work step carried out by the shot peening service provider. The aim is to determine machine parameters for the peening process so that compressive stresses are induced largely homogeneously and according to the depth profile required by the designer. This adjustment process includes shot peening with varied ball speeds, respectively conveying air pressures and e. g. the X-ray diffraction measurement of the residual stresses achieved.

Furthermore, the determination of the necessary peening time is part of the work step. For this purpose, the graph of the achieved **arc height of the Almen strip** $A(t)$ over the peening time is examined for saturation. The saturation time t_{sat} is characterized by a 10% increase in arc height while doubling of the peening time t_{peen}. The associated Almen arc height $A(t_{sat})$ is called Almen intensity $J_{<N/A/C>}$ (Almen strip types N, A, C). Due to its averaging character, the arc height is an integral statement on the saturation of the residual compressive stress field. Details on dimensions, material and measuring technique can be found in Refs. [12, 13].

The surface is checked for whether it is entirely impacted. For this purpose, the **coverage ratio** D is determined with the aid of a microscope and, if necessary, a fluorescent test liquid. The aim is to determine the saturation peening duration $t_{100\%}$, at which almost complete coverage ($D = 98\%$) is achieved. The maximum of the two times, the saturation time t_{sat} of arc height and the time for complete coverage $t_{100\%}$, is to be used for the process. In practical application, a multiple (typically 2) of the identified maximum peening duration is used. The coverage ratio is often the leading variable. For the overall validation of the shot peening, fatigue tests may be carried out.

1.2. Approaches of Simulation

Different approaches for the simulation of the shot peening process can be found in the literature. In Ref. [14], a sheet metal is modelled as a symmetry quarter of an Almen strip, which is shot peened in a small area around the center. The effect of vertical impacts on the residual stress is investigated for different ball diameters and velocities.

The coverage ratio D as a function of the number of impacted balls is the subject of the investigations in Ref. [15]. A small, central area of a circular plate is shot with randomly positioned balls. It is shown that the coverage ratio can be described by the Avrami equation. In Ref. [16], the influence of friction on the residual stress after oblique ball impacts is also investigated with a circular plate model and a random impact pattern. At an impact angle of 45°, a maximum value of the residual stresses is obtained over the coefficient of friction μ. This stress remains practically unchanged above $\mu = 0.3$. A beam model is used to calculate the arc height of the Almen strip caused by the residual stress field.

In Refs. [17–19], a cell model is employed that works with symmetry conditions on cell's boundaries. When a ball hits the cell close to its faces, unnatural results are obtained because of the interaction with the mirrored impact. Therefore, only certain regular impingement patterns have been used. The influence of the coefficient of friction on residual stress is examined in Ref. [17]. For coefficients in the range of $\mu = 0.1$ to

0.5, the effect is judged to be negligible for vertical impacts. In Ref. [18], a comparison of calculated residual stresses and stresses measured by X-ray diffraction is undertaken. Since the measurements average over a range, the calculated fields are averaged correspondingly for the purpose of comparison. Furthermore, the influence of the material model of the ball on the stresses calculated in the component is investigated. An elastic-plastic, an elastic and a rigid model are tested – the latter two without calibration to the case of the elastic-plastic ball.

Bending of the unit cell and hence rotation of the unit cell's boundaries against each other is treated in Ref. [20]. A generalization of periodic coupling conditions is displayed in Ref. [21]. It takes into account torsion and bending of the coupled cell's boundaries relative to each other. This paper shows a generalized approach taking into account rotation and translation of the unit cell's boundaries. This allows, beyond torsion and bending about an arbitrary axis, to account for expansion.

In Ref. [22], a particle simulation (Discrete Element Method) is used to simulate the ball flow after exiting the nozzle to investigate the interaction of the balls – moving towards the component or bouncing back – in the air flow. This determines the ball's impact locations and the distribution of the ball velocities.

2. Method – Modelling of the Shot Peening Process

2.1. Basic Model Properties

Model Requirements. The model shall be capable to represent both, the (thin) Almen strip which arches up due to residual stresses by shot peening as well as the (thick) component with its induced residual stress field experiencing negligible bending because of its thickness. Furthermore, it shall be possible to represent saturation effects in the residual stress with random impact patterns.

Also, the area-specific number of impacts to be simulated is a decisive factor, since it determines the computational manageability. The more balls, the greater the number of degrees of freedom for which the nonlinear system of equations must be solved each time step. To determine the *order of magnitude* of the number of area-specific impacts, a peening process described elaborately in Ref. [23] has been evaluated. Based on the data given there, an area-specific number of 700 balls/mm^2 is determined for double coverage, $2{\cdot}t_{100\%}$. An average ball diameter of 0.5 mm is underlying this number. In the present work, the underlying ball diameter is 0.8 mm, hence the area-specific number of balls converts to 300 balls/mm^2. A simulation-based verification is shown in Sec. 3.2.2.

This area-specific number will serve as the reference. At the chosen cell's edge length of 0.48 mm it results in a total of 70 impacts to be modelled, reflecting double coverage. On a typical office PC, this took about 30 h CPU time. An entire component could not be handled at all. The unit cell approach thus makes the simulation of shot peening with a realistic number of impacts accessible in the first place. The generalized constraints add capabilities to the unit cell formulation.

Key Data of the Model. The model is designed as a periodic unit cell. Hence, all its virtual repetitions experience the same history. Fig. 2 shows the finite element mesh of the unit cell and of the sphere. A convergence study has been carried out to determine mesh densities for the 20 node hexahedral elements with quadratic interpolation. Their edge length at the impacted surface of the unit cell results with 30 µm (16 × 16 elements, cell dimensions: 0.48 × 0.48 × 1.3 mm^3). For the surface linearly interpolated contact segments with half the element's edge length are applied on top (contactor). The sphere's potentially contacting area (target) is meshed equally sized at the center of contact, and aside up to two times larger using the same element and segment types. Areas of different mesh density in the unit cell are coupled with constraints at locations away from domains of local interest.

The transient calculations are performed with the implicit time integration scheme according to Bathe-Noh in the FEM program ADINA [24]. Displacement based elements are used having additional pressure degrees of freedom in favor of convergence in plasticity. Time steps in the different process periods (acceleration, impact, damping, see below) varying from 0.01 s to 0.1 µs are used. The underlying material, 40NiCrMo6, is used in aerospace engineering [25] and in automotive industry for structural, highly stressed components. The material is frequently subject to shot peening in these applications. Based on [16] the model assumes identical material for the Almen strip and the shot.

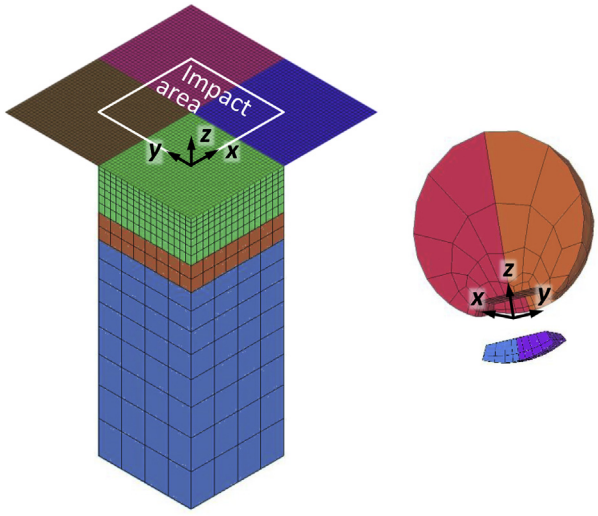

Fig. 2. Model of the unit cell, representing an Almen strip type A (0.48 × 0.48 × 1.3 mm^3), and of the sphere (Ø 0.8 mm). To represent a component, the thickness and mesh density of the unit cell can be adjusted. Above the unit cell there are four contact surfaces cyclically coupled to the solid elements. The targeted impact area is in the middle of the contact surfaces.

Due to the estimated specific number of impacts (300 balls/mm^2), only small surface areas can be handled in reasonable simulation time. However, there is a lower limit on cell size due to the range of influence of an impact. This should at least be completely contained in the modelled zone [26] so that it does not interact with its virtual neighbors. Thus, with a ball diameter of 0.8 mm, an impact velocity of 75 m/s and steel 40NiCrMo6 with a yield strength of $\sigma_y = 1510$ MPa (typical for Almen strip and shot [18]), an edge length of 0.48 mm of a square surface area is obtained by analysis. Results for vertical impacts are presented in the following.

Material Model. A multilinear plastic material model (J2 plasticity) with isotropic strain hardening is used for the component, for the Almen strip as well as for the balls, assuming large strains. The elastic material properties are: modulus of elasticity $E = 205$ GPa, density $\rho = 7850$ kg/m^3, Poisson's ratio $\nu = 0.25$, yield strength $\sigma_y = 1510$ MPa and a tangential modulus of 1200 GPa. The underlying stress-strain curve has been adopted from Ref. [16]. From this source, experimental shot peening data have been taken up for validation as well. Two linear sections appear sufficient to represent the elastic and hardening behavior. A comparison of two shot peening simulations with isotropic and mixed (70/30% isotropic/kinematic) hardening shows a difference of max. 3% in the compressive residual stress, averaged over the cell. A strain rate dependency of the flow curve is neglected. The temperature change is negligibly small, even for the Almen strip with its little mass.

Contact Model. Coulomb's law of friction with a constant coefficient of friction of $\mu = 0.6$ is applied between shot and unit cell. The comparatively high value takes account of the fact that intensive contact occurs during plastic deformation in the course of the impact/rebound. Relatively high maximum possible friction forces accompany the contact. Calculations for an impact angle of 90° to the surface show extensive invariance to the coefficient of friction, as also explained in Ref. [17]. The constraint equation algorithm is used to implement contact conditions.

Damping. The elastic energy remaining after plastic deformation leads to waves. Due to the limited volume of the unit cell model, the

waves would become stronger and stronger with further impacts. In reality, there is material damping and damping in fixations. Beyond that, away from the peening zone there is material capable to absorb and damp elastic waves. In consequence, there is no severe build-up of wave energy. To avoid the problem of increasing waves affecting impact process simulation, a damping step is inserted after each impact and all remaining wave energy is dissipated.

2.2. Generalized Cell Periodicity

The unit cell represents a section of the whole. The whole is obtained by repeated juxtaposition of the unit cell in two spatial directions. Since periodic coupling (rather than mirror) conditions are used, and the cell is sufficiently large, there are no artificial interactions between impacts on virtual neighbors. The unit cell has periodic couplings at its boundaries as well as at its surface covered with contact segments (Fig. 2, green top surface). Beyond the contact surface of the unit cell itself, there are three additional identical surfaces with contact segments only, which are periodically coupled with the unit cell. The targeted impact area at the size of one contact surface is located in the middle of all surfaces. This ensures proper impact on the unit cell. E. g., a ball contacting on the edge of the cell experiences contact to full extent. Periodic coupling of the additional contact surfaces propagates the cell's stiffness.

In the simplest case, the periodic coupling conditions at the cell's boundaries express the displacement vector of a point on one boundary to be identical to the vector on the opposite boundary at congruent position. This formulation, however, does not allow grasping the up-arching of the Almen strip driven by residual stresses after removing its fixation. Neither does it allow the application of pre-stresses. Due to periodicity, the coupled boundaries of the unit cell must have the same shape. In the process of up-arching or in the presence of pre-stress, they take up rotated and shifted positions relative to each other. The mentioned simple periodic coupling conditions cannot represent this.

In order to overcome this deficiency, the periodicity conditions are as illustrated in Fig. 3 and expressed as a vector coupling equation. This reads for e. g. node 3'

$$\boldsymbol{u}_3' = \boldsymbol{u}_3 + \boldsymbol{q} + \boldsymbol{\varphi} \times \boldsymbol{r}_{13}' \tag{1}$$

It has to be set up for each node pair of the boundaries to be coupled. In this equation $\boldsymbol{u}$ and $\boldsymbol{u}'$ are the displacement vectors of two congruent nodes. Furthermore, two **coupling variables** appear:

- the vector of relative displacement between coupled boundaries $\boldsymbol{q}$, e. g. an expansion due to, e. g., temperature change or tension,
- and the small rotation vector $\boldsymbol{\varphi}$, which describes the rotation of one boundary relative to the coupled one, e. g. due to residual stresses.

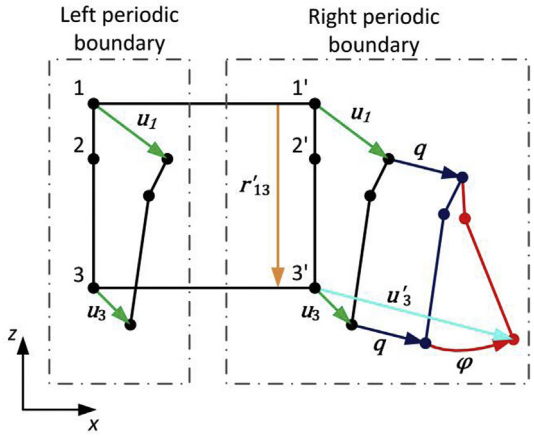

Fig. 3. Coupling of congruent nodes (1 to 3 and 1' to 3') of opposite periodic boundaries of the unit cell in such a way that the copy of the deformed shape of the left boundary merges into the deformed one of the right boundary by displacement $\boldsymbol{q}$ and rotation $\boldsymbol{\varphi}$.

Each of the four coupling variables is the same for all nodes of a coupled boundary pair. Each coupling variable is represented by the degrees of freedom of one additionally defined node. The vector $\boldsymbol{r}'$ is the position vector from a reference node of the primed boundary (node 1' in Fig. 3) to the coupling node of the same boundary. Thus, the cross product describes the small relative rotation of the periodic boundaries of the unit cell. This cell periodicity is implemented into the model with constraint equations as available in the finite element program. Simple tests such as pure bending about one and two axes have been carried out to verify the correctness. The generalized periodic coupling allows the representation of both, the component (usually thick and not deforming relevantly under residual stress) and the Almen strip (thin, arching up due to residual stress). This is an innovative kind of generalized periodic coupling to represent a unit cell. Its application to shot peening is novel.

The coupling equations also apply in *rotationally* periodic cases. Then, in at least one coupled pair of boundaries, these boundaries are situated under an angle of periodicity. The degrees of freedom to be coupled, $\boldsymbol{u}$ and $\boldsymbol{u}'$, have to be measured in coordinate systems rotated against each other by the angle of periodicity. Beyond that, in either case boundary pairs can have any shape as long as congruency is kept.

Use of the Coupling Variables. There are three basic applications of the unit cell: thick component, (thin) Almen strip and pre-stressed thick component. A **thick component** does not show (significant) expansion nor bending after shot peening. This is because the stiff bulk material under the thin layer of residual stress at the surface maintains the shape of the component. Consequently, the residual stresses in the thin layer are not significantly reduced by relieving the component from its fixation, if any. The unit cell represents a section of a thick component with a fraction of its thickness. Therefore, to represent the non-expanding and non-bending behavior, the cell's expansion $\boldsymbol{q}$ and rotation $\boldsymbol{\varphi}$ are set to zero during and after shot peening.

An **Almen strip**, unlike the thick component, arches up after peening, once released from its holder. Representing an Almen strip, the cell has the original thickness and is fixed on its underside during the peening simulation; the coupling variables are free. After removal of the fixation, the values for the coupling variables adjust freely according to the residual compressive stresses. From the rotations $\boldsymbol{\varphi}$ of the two periodic boundary couplings the arching up about the x- and y-axis can be calculated for the unit cell and in turn for the Almen strip. To yield the entire arc height of the Almen strip A the two results are superimposed. Some of the coordinates of $\boldsymbol{\varphi}^x = \left(\varphi_x^x,\ \varphi_y^x,\ \varphi_z^x\right)$ for the coupling of the boundaries having a normal parallel to the x-axis, Fig. 3, are found to be negligibly small, i. e. only φ_y^x is relevant. The relevant rotation for the other pair of periodic boundaries is the same by amount because of isotropy, $\left|\varphi_y^x\right| = \left|\varphi_x^y\right|$. Beyond that, the expansions $\boldsymbol{q}^x$ and $\boldsymbol{q}^y$ are found to be negligibly small as well. The support distances on the Almen gage are $L_1 = 31.75$ mm and $L_2 = 15.85$ mm (SAE J442). Based on this, the arc height results from

$$A\left(\varphi_y^x, \varphi_x^y\right) = R^x\left[1 - \sqrt{1 - \frac{L_1^2}{4\left(R^x\right)^2}}\right] + R^y\left[1 - \sqrt{1 - \frac{L_2^2}{4\left(R^y\right)^2}}\right] \tag{2}$$

with $R^x = L_u/\left|\varphi_y^x\right|$ and $R^y = L_u/\left|\varphi_x^y\right|$ being the curvature radii in which $L_u = 0.48$ mm is the edge length of the square unit cell. This formula captures the two-dimensional curvature [27].

The simulation of **shot peening under component pre-stressing** is basically similar to the simulation without pre-stress described above for the thick component. The expansion $\boldsymbol{q}$ and rotation $\boldsymbol{\varphi}$ are assigned values that correspond to the intended pre-stress. After shot peening the component is relieved from the pre-stress. It nearly returns to its original

shape because of the stiff bulk material. This is modelled by resetting the coupling variables to zero.

3. Results and Discussion

First, the integral and local saturation behavior of the residual stresses, rarely displayed in the literature, are discussed. Afterwards the main control parameters for quality assurance of the shot peening process, the arc height of the Almen strip and the coverage, are considered. A validation of the generalized constraints is displayed employing measured arc height. Finally, an application for shot peening under pre-stress is presented.

3.1. Characterization of the Residual Stress Field

3.1.1. Basic Characterization

For the evaluation of residual stress the pressure σ_p is used, which is the negated hydrostatic stress σ_h of the stress tensor $\boldsymbol{\sigma}$, $\sigma_p = -\sigma_h = -1/3\,\mathrm{tr}(\boldsymbol{\sigma})$. This quantity was chosen because it is the most important parameter for fatigue behavior in the context of surface strengthening. Various fatigue criteria refer to the pressure to capture the mean stress influence [28, 29]. The calculation shows second and third principal stresses to be approximately the same and parallel to the surface. It is therefore irrelevant which orientation a surface fatigue crack might have. This appears different for shot peening under pre-stress. The first principal stress is comparatively close to zero. It points perpendicular to the surface.

3.1.2. Integral Consideration

In sections placed parallel to the surface of the unit cell at different depths z, mean values and standard deviations of the pressure σ_p are evaluated for the unit cell's cross section. The results are determined over all $16 \times 16 = 256$ element faces of this section, Fig. 2, and are displayed over the number of impacts. An extract from this evaluation is shown in Fig. 4 for the section in which the final maximum of the mean compressive stress over the entire section is reached, z = -64 µm. The mean value of the pressure in this selected section increases with progressing number of impingements, while the standard deviation decreases. An extrapolation shows an increase of the mean value by 5% and a reduction of the standard deviation by 14% with a doubling of the number of impacts to 140. According to the 10% saturation rule for the arc height of the Almen strip, seven balls are sufficient; according to the simulation of the coverage ratio D, Section 3.2.2, 46 balls per unit cell are sufficient for double coverage, $2{\cdot}t_{100\%}$. With the practically used double coverage the standard deviation of the pressure is still around 11% of the mean value or 125 MPa.

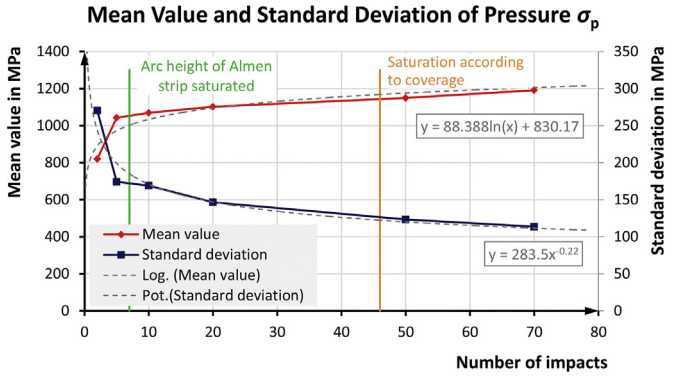

Fig. 4. The mean value and standard deviation of the pressure σ_p of the section z = -64 µm over the number of impacts. The process can be terminated after 46 impacts on the unit cell for double coverage, corresponding to 200 balls/mm^2.

3.1.3. Local Stress Field

So far, the scatter of the entire cell's cross-section has been presented as an *integral* characterization, i. e. by its statistics. In the following, the *local* development of the pressure in the course of the peening process is considered. Fig. 5 shows the pressure σ_p in the same section as before, z = -64 µm, after the 66th and 67th impact. As expected, a high pressure results at the location of the 66th ball after its impact. At that time, the pressure at the location of the 67th ball is comparatively low. After impact of ball 67, as expected there is higher pressure. However, at location of ball 66 the pressure decreased again. This may be explained by strains due to impact of ball 67 extending to location 66. Supported by evaluations of accumulated plastic strain it is assumed that reverse plastification has been caused at position 66 due to impact 67. Because of re-shortening of fibers, pressure has reduced. Concluding, locally the pressure field does not increase monotonously from impact to impact; rather there is an ongoing variability. This can also be observed looking at individual element faces that are evaluated over the number of impacts, Fig. 6. Even after a large number of impacts beyond saturation in coverage at 46 hits, fluctuations of more than 400 MPa are displayed. The extent of hills and troughs obviously exceeds the grain size, Fig. 5. In consequence the variations are fatigue relevant. A corresponding behavior can as well be observed in section planes perpendicular to the surface.

Significance of Local Stress Field. The effect just presented is rarely described and analyzed in the literature. In Ref. [30], comparable stress patterns are presented, but their scatter is not discussed. The significance of the local values results from the fact that the weakest compressive stress has the least positive influence on material fatigue (weakest link). It therefore must be taken into account when determining the fatigue life. The described local variation of the pressure continues beyond the technically meaningful range of number of impacts. This behavior is evidenced both by the low rate of change of the standard deviation, Fig. 4, and by the local behavior, Fig. 6. In the application, the process is terminated when the desired degree of coverage and a stationary arc height are reached. Then the scatter of the local pressure is still significant. The residual stress field in Fig. 5 shows a span of about 40% of its mean value, though the saturation point $t_{200\%}$ (46 impacts) has already been exceeded.

An X-ray diffraction measurement of the pressure averages over a spot of the size down to 30 µm, depending on equipment [31]. This allows the inhomogeneity of the pressure field to be determined by measurement.

Of course, it makes no sense to look for the minimum pressure on a scale below the grain size of the material in the fatigue assessment, since then the usability of the continuum mechanical model is no longer given. Instead, the principle of critical distances [32] can be followed, taking into account the scatter. According to this, fatigue is governed by stress averaged over a small distance, area or volume around the potential crack initiation site. The critical distance's size is of the order of magnitude of the grain size. The stresses averaged over each element face of 30 × 30 µm (being at the order of magnitude of critical distance) show standard deviations in the order of 10% of their mean. The stress field thus averaged is to be evaluated for fatigue.

3.1.4. Conclusions on the Residual Stress Field

Integral Evaluation. The integral evaluation of the residual stress field shows saturation. However, even with double coverage, $2{\cdot}t_{100\%}$, the pressure field is characterized by an appreciable standard deviation in the order of 10%, Fig. 4.

Local Stress Field. The local residual stresses are decisive for the fatigue behavior within a surrounding of the size of the equivalent structural area [32]. These stresses do not show saturation within the technically meaningful range of impacts, Fig. 6. Since the accumulated strain introduced must not be too high due to low cycle fatigue [33], peening cannot be continued for any length of time. So a homogeneous

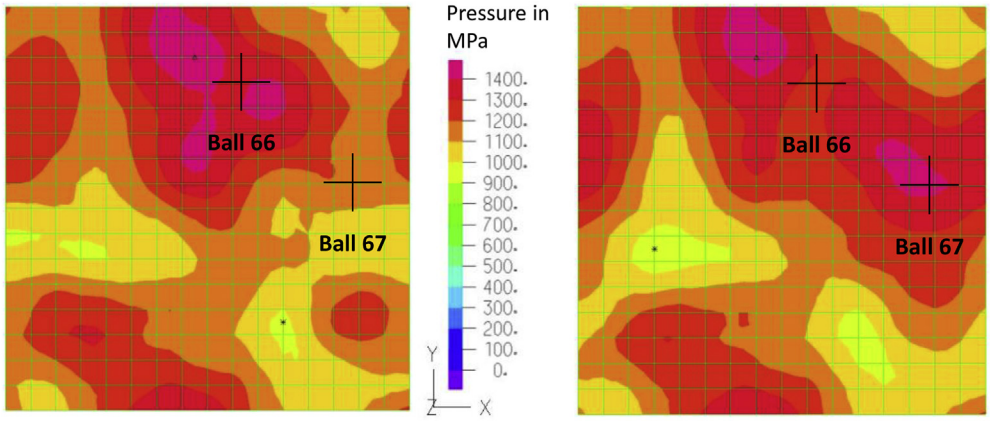

Fig. 5. Pressure in surface-parallel section, z = -64 µm, mesh size: 30 µm. Influence of successive impacts on the pressure field; left: after ball 66, right: after ball 67. In this example, the total range of variation over the unit cell is about 500 MPa, i. e. about 40% of the mean value.

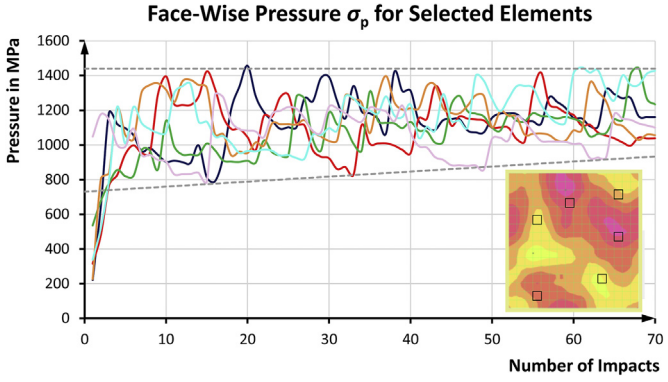

Fig. 6. Graph of local pressure σ_p on faces of selected elements in section at z = -64 µm over the number of impacts. E. g., the red curve comes down from 1400 MPa after 56 impacts to 1000 MPa after 67 impacts.

pressure field cannot be achieved economically, a certain amount of scatter remains. It is advisable to consider this scatter behavior in fatigue evaluations.

3.2. Validation

3.2.1. Arc Height of the Almen Strip – Comparison to Measurement

Basis of Comparison: Unit Cell. The arc height of the Almen strip can be calculated from the rotations φ of the two periodic boundary couplings according to Eq. (2). For a comparison with other authors, the Almen intensity J_A according to the 10% saturation rule is not considered here. Instead, the arc height A_S after a large number of impacts in the saturation range is used, because this is more reliable due to its stationarity. Fig. 7 shows the graph of the arc height A vs. the number of impacts for a type A Almen strip according to simulation. The saturation point following the 10% rule results after a few impacts. At 75 m/s impact velocity, the saturation value of the arc height is $A_S = 0.5$ mm.

Comparison with Arc Height from Shell Model. The residual stresses obtained from the unit cell model representing a flat fixed Almen strip can be integrated over the x-/y-normal unit cell boundaries to obtain the effective moment. For comparison with the arc height determined with rotations φ, a shell model is used. This represents a not peened Almen strip at whose free edges the determined moment is introduced. An elastic calculation yields the arc height. Unit cell and shell model provide practically identical values (deviation $< 0.5\%$). This means that actually present boundary effects of the domain-wise limited Almen strip are negligible compared to the unit cell, which represents an infinite sheet.

Comparison with Beam Model. The use of a beam model to estimate the arc height of the Almen strip due to residual stresses by imposing the bending moment to the beam's ends is common. This model, however, cannot take into account the stiffening curvature in the transverse direction of the Almen strip as well as the deflection in the transverse direction. As a result, the beam model overestimates the arc height by 7% for the type A Almen strip. This deviation is *systematic* due to the linearity between moment and arc height.

Comparison with Measured Arc Heights. The points in the graph of Fig. 8 are measured values of the arc height for various shot velocities, Refs. [16] Tab. 1, [18]. The shot velocities were determined by the authors of [18] indirectly from the measured arc height using the beam model. In view of the systematic overestimation of the arc height by 7%, the curves have been corrected downwards. Furthermore, for the shot velocity of 75 m/s, underlying the present work, a curve was obtained by slight extrapolation of the measured data. This is shown in Fig. 8 including the correction of the overestimation, also for the case of 40 m/s (dashed lines). In addition, the saturation values of the arc height obtained with the unit cell for the two shot velocities are displayed there. It is stated in Ref. [16] that the examined peening times are a multiple of $t_{100\%}$. Therefore, the right area of the diagram is to be considered for a comparison. A good agreement can be recognized with a maximum deviation of about 6% in the case of 40 m/s.

3.2.2. Coverage Ratio – Comparison to Shot Peening Treatment Evaluated in Sec. 2.1

In Sec. 2.1, a shot peening treatment was examined, in which 300 impacts/mm^2 at $t_{200\%}$ were found as a representative estimation. To further underpin this value, it will be verified by simulation in the following.

The Coverage ratio D indicates the proportion of the total area hit by balls, Fig. 9 top left. A Monte Carlo simulation has been carried out to determine this ratio. It is based on a constant area-specific shot flow $\dot{V}_s$ in pieces/(mm^2 s). Each impact causes an impression on the unit cell. The sizes of the partially overlapping impressions are taken from the finite element analyses. The observed variation in diameter of the overlapping hits is small at approx. 3%. The mean value is used in the Monte Carlo simulation as a constant impression size. As the number of shots increases, the area covered increases. The graph of the covered area over time or over the number of impacts allows the determination of the number of impacts required for 98% coverage. This is nominally referred to as 100% coverage. One hundred of such Monte Carlo experiments lead to the frequency distribution shown in Fig. 9. It indicates the number of impacts by which 98% coverage is achieved in the simulation: On average 23 impacts on the unit cell of 0.48^2 mm^2, corresponding to the peening time $t_{100\%}$ for quasi 100% coverage. The peening time frequently

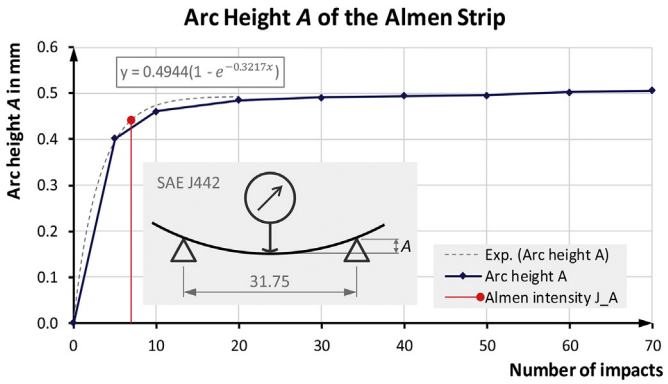

Fig. 7. Arc height A of the Almen strip in the course of the ball impacts according to simulation. The saturation point (red) results from the 10% rule.

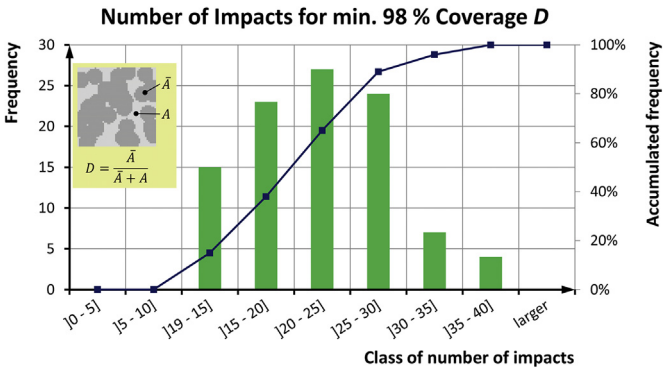

Fig. 9. To reach 98% coverage, the number of impacts as indicated on the horizontal axis have been necessary in a number of Monte Carlo experiments indicated on the vertical axis. The mean value is 23 balls for the unit cell. This corresponds to the peening time $t_{100\%}$ for quasi 100% coverage.

used in practice of $t_{200\%} = 2{\cdot}t_{100\%}$ corresponds here to 46 impacts on the unit cell or 200 impacts/mm^2, which very probably ensures 100% coverage. Concluding, this value and the value resulting from the estimation described in Section 2.1 are in agreement.

3.3. Application – Shot Peening under Pre-Stress

Procedure. Shot peening with pre-stressing of the component opens up further potential of the process. Thus, the stress profile of pressure in the part can be improved. During the peening process, the component is loaded and fixed in such a way that a tensile stress is created in the direction of the later stress caused by the service load. The pre-stress is in the order of magnitude of the yield strength. After peening, the load for the pre-stress is removed. The generated residual stress field is not isotropic due to the directional pre-stress field. Its anisotropy is such that its superposition with the stress due to service load results in a lower mean stress compared to shot peening without pre-stress. This process is used for springs and turbine blades, among other applications. [2, 34]

Component Simulation. The unit cell model with the generalized cell periodicity allows to impose deformations representative for pre-stressing. Two examples:

- A unidirectional pre-stress, as experienced e. g. by a component under tension and/or bending, can be represented by the coupling equation (1) of the unit cell. For tension, a relative displacement $\boldsymbol{q}$ is impressed between *one* coupled pair of boundaries; for bending, a relative rotation $\boldsymbol{\varphi}$ is additionally impressed. The coupling variables of the other pair are set to zero (plane strain), Fig. 10 left. These kinematic constraints trigger the stress field typical for tension and/or bending in the unit cell. With this stress field in place the shot peening is simulated.
- The torsional pre-load of a coil spring can be represented as bidirectional pre-stress. Thereby two principal stresses of the same magnitude and opposite sign with a linear decline to the center of the wire's cross section are used. Thus, two equally large relative angles $\boldsymbol{\varphi}$ and two displacements $\boldsymbol{q}$, each of opposite sign, are to be imposed to the unit cell boundary pairs each with the coupling equation (1), Fig. 10 right.

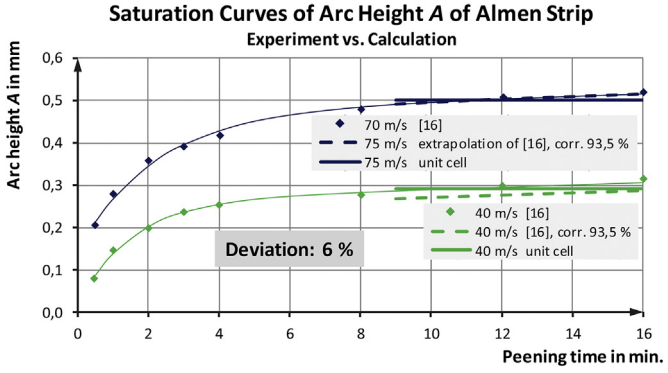

Fig. 8. Saturation curves based on measurements compared to the results of the unit cell. The points represent the original readings from Ref. [16], Tab. 1. The dashed lines are measured data, reduced by the inherent overestimation of the original data, and in case of 75 m/s extrapolated from 70 m/s. The solid lines represent the values after 70 impacts on the unit cell models.

The constraints are kept constant during the simulation of the peening process in order to reflect component fixation. To remove the pre-stressing, rotation $\boldsymbol{\varphi}$ and expansion $\boldsymbol{q}$ are set to zero, since the thin residual stress layer at the surface is mostly returned to its original shape due to the dominating elastic bulk material underneath.

Because of the thin layer created by shot peening there are applications, which may neglect the stress gradient in the pre-stress. Then, imposing a constant stress via expansion $\boldsymbol{q}$ is sufficient. Oppositely, at notches there may be a stress gradient leading to relevant stress reduction within the expected residual stress layer. In that case, rotation $\boldsymbol{\varphi}$ can reflect the stress gradient.

Results. In the following, results for **bending pre-stress** about the x-axis are displayed. The peening parameters are identical to those in Section 3.1 and 3.2 to allow comparison. The small number of ten balls is used leading to a simulation time of 4.5 h (including the load relieving). Fig. 4 gives an idea of the moderate deviations from quasi-saturated state in average pressure and its standard deviation to be expected.

In sections placed parallel to the surface of the unit cell at different depths z, mean values and standard deviations of the residual stress in direction of the load stress σ_{yy} are evaluated. Two different levels of pre-stress are used for this analysis.

As long as the pre-stressing is maintained, the **mean residual stress** curve is largely the same from the surface to the end of the compression plateau, compared to the non-pre-stressed case, Fig. 11. After removal of the pre-load, an increased residual compressive stress field is in place. This is due to the fibers, prolonged by the peening process. These experience stronger compressing in direction of the service load, which was the direction of the pre-stressing. In addition, the width of the plateau increases towards the surface as well as into depth. For 88% pre-stress, as percentage of yield strength, the plateau shows an expansion to ≈200% in width and an increase to ≈120% in stress. The **standard deviation** appears to be lower in the residual stress plateau for the pre-stressed case. It is around half to two third of the non-pre-stressed case.

Torsional pre-stressing has been investigated at comparable level of

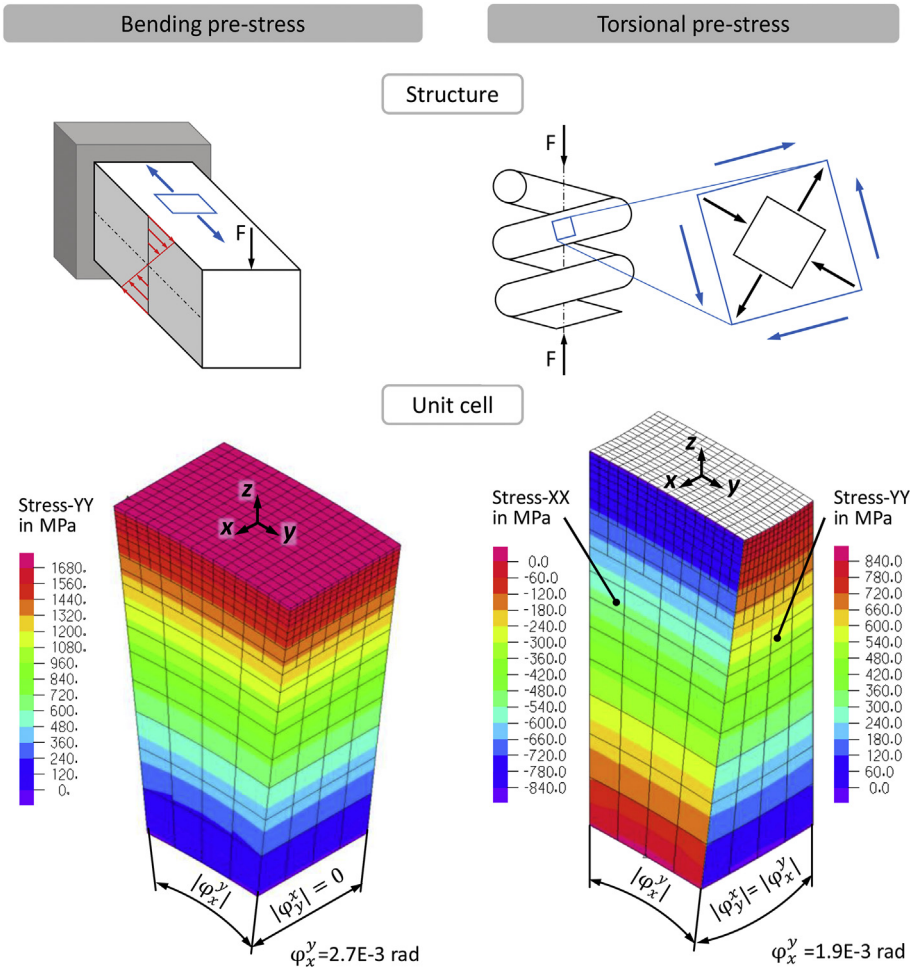

Fig. 10. Left: Pre-stressing for bending about the *x*-axis. Here, the bottom of the unit cell is at the neutral plane of the beam. Right: The torsion of an element on a coil spring is shear stress free at 45° to the wire axis (top right). Therefore, it can be simulated with the unit cell by imposing two opposite principal stresses. In both cases (bending and torsion) the maximum von Mises stress is defined slightly below yield strength.

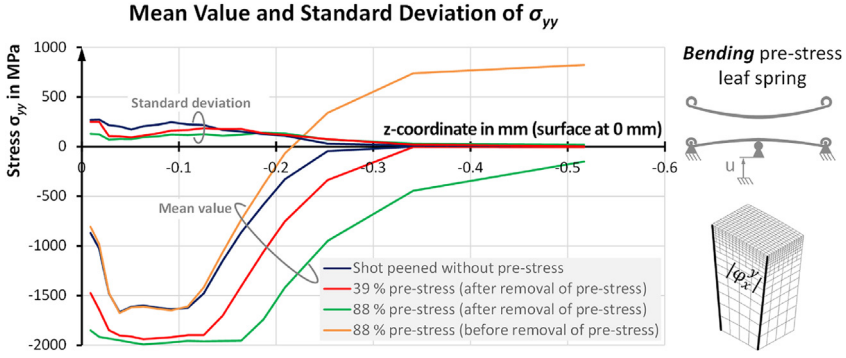

Fig. 11. Influence of the unidirectional pre-load in *y*-direction on the corresponding residual stress σ_{yy} before and after removal of the pre-stress, evaluated in cut planes at depth *z*. Given pre-stress is von Mises stress as percentage of the yield stress. Results shown are after ten impacts.

detail. Since shot peening only affects the upper layer of the material and the gradient of pre-stress is moderate, a unit cell with a fraction of the radius of a coil spring's wire would be sufficient. However, to reflect waves traveling away before they reflect, return, and possibly interact with the ball still in contact, the unit cell has simply been prolonged neglecting the conical shape downwards to the wire's center. The cell's height is chosen to be the radius of the wire.

The pre-stress in the upper layer, which is thus imposed with two relative angles $\boldsymbol{\varphi}$, is the same as chosen in the bending case, 88% of yield. The results in averaged stress and scatter in direction of the load are in general fairly equal to the shown case of bending. The benefitting direction is that of the tensile principle stress.

4. Conclusions

An efficient unit cell model employing a generalized cell periodicity allowing for relative displacement and rotation of the coupled periodic boundaries has been developed and applied to the shot peening process.

Its advantages are in the ability to either prescribe expansion, shear, bending and twist or to read out these quantities as results. This may even switch during analysis. For example, the up-arching of the Almen strip can be calculated from the resulting cell's bending angles.

The unit cell has been validated based on measured arc heights available in the literature for two clearly different shot velocities. The scatter in residual stress was demonstrated to virtually not diminish below a final value with increasing peening time. Scatter hence should enter design calculations rather than averaged values only.

Furthermore, the prescription of deformation has been demonstrated for simulation of shot peening under pre-stressing by bending. The obtained results confirm higher levels and greater depth of the compressive stress layer. Another application with torsional pre-stress, as met with shot peening of coil springs confirms that as well.

With regard to the corporate process of shot peening the simulation allows to consider a simplification in the adjustment of the peening apparatus. Using the predicted arc height as means of specification instead of the residual stress field eliminates the need for an iterative adjustment procedure. Hence, it is possible to eliminate or reduce the involved repeated costly residual stress measurements. Beyond that, because of the simulation approach for specification of shot peening, the properties of the residual stress field are known at an early design stage.

Funding Information

This research did not receive any specific grant from funding agencies in the public, commercial, or not-for-profit sectors.

Authors' Contributions

C. H. Richter contributed the idea of the generalized coupling, supervised the work and wrote large parts of the publication. P. Gerken developed the model, carried out simulations and validation. He wrote large parts of the publication. G. Telljohann provided input from his experience with simulation of strengthening by hammering. He also proof-read the manuscript.

Data Availability

The measured data required to reproduce presented findings of Sec. 3.2.1 were extracted from the work of Kim et al. [16], Tab. 1.

Declaration of Competing Interest

The authors declare that they have no known competing financial interests or personal relationships that could have appeared to influence the work reported in this paper.

References

[1] J. Kritzler, W. Wübbenhorst, Inducing Compressive Stresses through Controlled Shot Peening, Handb. Residual Stress and Deformation of Steel, 2002, pp. 345–358.
[2] Curtiss-Wright Surface Technologies, Surface technologies – shot peening applications. www.cwst.de, 2016. (Accessed 23 September 2019).
[3] R. Wagener, M. Hell, T. Melz, Anforderungen an ein Bemessungskonzept für zyklisch beanspruchte additiv gefertigte Bauteile, in: H.A. Richard, B. Schramm, T. Zipsner (Eds.), Additive Fertigung von Bauteilen und Strukturen, Wiesbaden, Springer Vieweg, 2017, pp. 227–240, https://doi.org/10.1007/978-3-658-17780-5_15.
[4] A.H. Maamoun, M.A. Elbestawi, S.C. Veldhuis, Influence of shot peening on AlSi10Mg parts fabricated by additive manufacturing, J. Manuf. Mater. Process. 2 (3) (2018), https://doi.org/10.3390/jmmp2030040.
[5] V. Schneidau, Strahlen von Stahl - Merkblatt 212. https://www.stahl-online.de/wp-content/uploads/2013/10/MB-212-Strahlen-von-Stahl.pdf, 2010. (Accessed 23 September 2019).
[6] D. Kirk, Size and variability of cast steel shot particles, Shot Peener 23 (2009) 24–32.
[7] D. Wu, C. Yao, D. Zhang, Surface characterization of Ti1023 alloy shot peened by cast steel and ceramic shot, Adv. Mech. Eng. 9 (2017) 1–14, https://doi.org/10.1177/1687814017723287.
[8] F.P. Zimmerli, Shot blasting and its effects on fatigue life, Surface Treatment of Metals (1941) 261–278.
[9] J.O. Almen, Peened surfaces improve endurance of machine parts, Metal Prog 43 (2) (1943) 209–315.
[10] T.L. Anderson, Fracture Mechanics - Fundamentals and Applications, fourth ed., Taylor & Francis Inc., Boca Raton, Florida, 2017.
[11] Saarstahl, Werkstoff-datenblatt SAE 1070. http://www.saarstahl.de/sag/de/produkte/index.shtml, 2019. (Accessed 23 September 2019).
[12] Standard SAE J442 August 2017: Test Strip, Holder, and Gage for Shot Peening.
[13] Standard SAE J443 August 2017: Procedures for Using Standard Shot Peening Test Strip.
[14] M. Guagliano, Relating Almen intensity to residual stresses induced by shot peening – a numerical approach, J. Mater. Process. Technol. 110 (3) (2001) 277–286, https://doi.org/10.1016/S0924-0136(00)00893-1.
[15] S.M.H. Gangaraj, M. Guagliano, G.H. Farrahi, An approach to relate shot peening finite element simulation to the actual coverage, Surf. Coating. Technol. 243 (2014) 39–45, https://doi.org/10.1016/j.surfcoat.2012.03.057.
[16] T. Kim, H. Lee, H.G. Hyun, S. Jung, Effects of Rayleigh damping, friction and rate-dependency on 3D residual stress simulation of angled shot peening, Mater. Des. 46 (2013) 26–37, https://doi.org/10.1016/j.matdes.2012.09.030.
[17] S.A. Meguid, G. Shagal, J.C. Stranart, 3D FE analysis of peening of strain-rate sensitive materials using multiple impingment model, Int. J. Impact Eng. 27 (2002) 119–134, https://doi.org/10.1016/S0734-743X(01)00043-4.
[18] T. Kim, J.H. Lee, H. Lee, S.K. Cheong, An area-average approach to peening residual stress under multi-impacts using a three-dimensional symmetry-cell finite element model with plastic shots, Mater. Des. 31 (1) (2010) 50–59, https://doi.org/10.1016/j.matdes.2009.07.032.
[19] G.H. Majzoobi, R. Azizi, A.A. Nia, A three-dimensional simulation of shot peening process using multiple shot impact, J. Mater. Process. Technol. 164–165 (2005) 1226–1234, https://doi.org/10.1016/j.jmatprotec.2005.02.139.
[20] J. Feng, Z. Xia, C. Zhou, Repeated unit cell (RUC) approach for pure bending analysis of coronary stents, Comput. Methods Biomech. Biomed. Eng. 11 (4) (2008) 419–431.
[21] Wei Cai, et al., Torsion and bending periodic boundary conditions for modeling the intrinsic strength of nanowires, J. Mech. Phys. Solid. 56 (11) (2008) 3242–3258.
[22] T. Hong, J.Y. Ooi, J. Favier, B. Shaw, A numerical simulation to relate the shot peening process parameters to the induced residual stresses, Eng. Fail. Anal. 15 (8) (2008) 1097–1110, https://doi.org/10.1016/j.engfailanal.2007.11.017.
[23] Abrasive Oberflächentechnik Sinning, Messung der Almenintensität - Kugelstrahlen auf einen Almenwert von 0,3 mm A. https://www.oberflaeche.com/blog/messung-der-almenintensitaet.html, n.y, (accessed 23 September 2019).
[24] R&D Inc ADINA, ADINA Theory and Modeling Guide - Volume I: ADINA Solids & Structures, 71 Elton Avenue Watertown, ADINA R&D Inc., MA 02472 USA, 2018.
[25] M.A.S. Torres, H.J.C. Voorwald, An evaluation of shot peening, residual stress and stress relaxation on the fatigue life of AISI 4340 steel, Int. J. Fatig. 24 (8) (2002) 877–886, https://doi.org/10.1016/S0142-1123(01)00205-5.
[26] T. Spradlin, R. Grandhi, K. Langer, Modified symmetry cell approach for simulation of surface enhancement over large scale structures, Conf. Proc. Int. Conf. Shot Peening. 11 (2011) 111–116.
[27] OSK-Kiefer GmbH, Qualitätskontrolle beim Kugelstrahlen. https://osk-kiefer.de/wp-content/uploads/Qualitaetskontrolle-und-Qualitaetssicherung_go.pdf,n.y. (Accessed 23 September 2019).
[28] R. Rennert, Rechnerischer Festigkeitsnachweis für Maschinenbauteile aus Stahl, Eisenguss- und Aluminiumwerkstoffen, sixth ed., Frankfurt, Verband Deutscher Maschinen- und Anlagenbau (VDMA) and Forschungskuratorium Maschinenbau (FKM), 2012.
[29] R.I. Stephens, A. Fatemi, R.R. Stephens, H.O. Fuchs, Metal Fatigue in Engineering, second ed., John Wiley & Sons, New York, 2001.
[30] T.Q. Pham, D. Butler, New approach to estimate coverage parameter in 3D FEM shot peening simulation, Surf. Eng. 33 (9) (2017) 687–695, https://doi.org/10.1080/02670844.2016.1274536.
[31] J. Bauch, R. Rosenkranz, Physikalische Werkstoffdiagnostik - Ein Kompendium wichtiger Analytikmethoden für Ingenieure und Physiker, first ed., Springer Vieweg, Berlin, 2017 https://doi.org/10.1007/978-3-662-53952-1.
[32] D. Taylor, The Theory of Critical Distances - A New Perspective in Fracture Mechanics, first ed., Elsevier Science, Oxford, 2010.
[33] M. Frija, T. Hassine, R. Fathallah, C. Bouraoui, A. Dogui, Finite element modelling of shot peening process: prediction of the compressive residual stresses, the plastic deformation and the surface integrity, Mater. Sci. Eng. 426 (1–2) (2006) 173–180, https://doi.org/10.1016/j.msea.2006.03.097.
[34] W. Koenecke, N.K. Burrell, C. Mehelich, Shot Peening Springs, 1982. Springs.